

Comparative Analysis of miRNA Expression after Whole-Body Irradiation Across Three Strains of Mice

Authors: Martello, Shannon, Bylicky, Michelle A., Shankavaram, Uma, May, Jared M., Chopra, Sunita, et al.

Source: Radiation Research, 200(3) : 266-280

Published By: Radiation Research Society

URL: <https://doi.org/10.1667/RADE-23-00007.1>

The BioOne Digital Library (<https://bioone.org/>) provides worldwide distribution for more than 580 journals and eBooks from BioOne's community of over 150 nonprofit societies, research institutions, and university presses in the biological, ecological, and environmental sciences. The BioOne Digital Library encompasses the flagship aggregation BioOne Complete (<https://bioone.org/subscribe>), the BioOne Complete Archive (<https://bioone.org/archive>), and the BioOne eBooks program offerings ESA eBook Collection (<https://bioone.org/esa-ebooks>) and CSIRO Publishing BioSelect Collection (<https://bioone.org/csiro-ebooks>).

Your use of this PDF, the BioOne Digital Library, and all posted and associated content indicates your acceptance of BioOne's Terms of Use, available at www.bioone.org/terms-of-use.

Usage of BioOne Digital Library content is strictly limited to personal, educational, and non-commercial use. Commercial inquiries or rights and permissions requests should be directed to the individual publisher as copyright holder.

BioOne is an innovative nonprofit that sees sustainable scholarly publishing as an inherently collaborative enterprise connecting authors, nonprofit publishers, academic institutions, research libraries, and research funders in the common goal of maximizing access to critical research.

Comparative Analysis of miRNA Expression after Whole-Body Irradiation Across Three Strains of Mice

Shannon Martello,^{a,1} Michelle A. Bylicky,^{a,1} Uma Shankavaram,^a Jared M. May,^a Sunita Chopra,^a Mary Sproull,^a Kevin MK Scott,^a Molykutty J. Aryankalayil,^{a,2} C. Norman Coleman^{a,b}

^a Radiation Oncology Branch, Center for Cancer Research and ^b Radiation Research Program, National Cancer Institute, National Institutes of Health, Rockville, Maryland 20850

Martello S, Bylicky MA, Shankavaram U, May JM, Chopra S, Sproull M, Scott KMK, Aryankalayil MJ, Coleman CN. Comparative Analysis of miRNA Expression after Whole-Body Irradiation Across Three Strains of Mice. *Radiat Res.* 200, 266–280 (2023).

Whole- or partial-body exposure to ionizing radiation damages major organ systems, leading to dysfunction on both acute and chronic timescales. Radiation medical countermeasures can mitigate acute damages and may delay chronic effects when delivered within days after exposure. However, in the event of widespread radiation exposure, there will inevitably be scarce resources with limited countermeasures to distribute among the affected population. Radiation biodosimetry is necessary to separate exposed from unexposed victims and determine those who requires the most urgent care. Blood-based, microRNA signatures have great potential for biodosimetry, but the affected population in such a situation will be genetically heterogeneous and have varying miRNA responses to radiation. Thus, there is a need to understand differences in radiation-induced miRNA expression across different genetic backgrounds to develop a robust signature. We used inbred mouse strains C3H/HeJ and BALB/c mice to determine how accurate miRNA in blood would be in developing markers for radiation vs. no radiation, low dose (1 Gy, 2 Gy) vs. high dose (4 Gy, 8 Gy), and high risk (8 Gy) vs. low risk (1 Gy, 2 Gy, 4 Gy). Mice were exposed to whole-body doses of 0 Gy, 1 Gy, 2 Gy, 4 Gy, or 8 Gy of X rays. MiRNA expression changes were identified using NanoString nCounter panels on blood RNA collected 1, 2, 3 or 7 days postirradiation. Overall, C3H/HeJ mice had more differentially expressed miRNAs across all doses and timepoints than BALB/c mice. The highest amount of differential expression occurred at days 2 and 3 postirradiation for both strains. Comparison of C3H/HeJ and BALB/c expression profiles to those previously identified in C57BL/6 mice revealed 12 miRNAs that were commonly expressed across all three strains, only one of which, miR-340-5p, displayed a consistent regulation pattern in all three miRNA data. Notably multiple Let-7 family members predicted high-

dose and high-risk radiation exposure (Let-7a, Let-7f, Let-7e, Let-7g, and Let-7d). KEGG pathway analysis demonstrated involvement of these predicted miRNAs in pathways related to: Fatty acid metabolism, Lysine degradation and FoxO signaling. These findings indicate differences in the miRNA response to radiation across various genetic backgrounds, and highlights key similarities, which we exploited to discover miRNAs that predict radiation exposure. Our study demonstrates the need and the utility of including multiple animal strains in developing and validating biodosimetry diagnostic signatures. From this data, we developed highly accurate miRNA signatures capable of predicting exposed and unexposed subjects within a genetically heterogeneous population as quickly as 24 h of exposure to radiation. © 2023 by Radiation Research Society

INTRODUCTION

Acute whole-body exposure to even moderate doses of ionizing radiation (>1 Gy) damages all cell types and can lead to acute radiation syndrome (ARS) that manifests in multiple organ systems (1–3). Survival permitting, untreated ARS can cause delayed effects of acute radiation exposure (DEARE) such as heart and lung fibrosis, as well as radiation-induced cancers (4, 5), in the months to years after exposure. Delivery of medical countermeasures within 24 to 48 h postirradiation may confer not only a survival advantage from ARS but may delay the onset of DEARE. However, in the event of widespread exposure from a radiological disaster (e.g., nuclear reactor accident, dirty bomb explosion or nuclear detonation), there will likely be scarce resources and insufficient countermeasures, necessitating a method to inform medical decision-making and efficiently distribute limited resources (6).

Radiation biodosimetry correlates biological changes with a physical dose of radiation and is used to guide triage and allocation of resources in a widespread exposure situation (7, 8). The current gold standard for biodosimetry is the dicentric chromosome assay (DCA). While DCA has demonstrated utility through its use in previous events like Chernobyl and Fukushima (9–11), its time-to-result and

¹ Scholar in training.

² Correspondence should be addressed to: Molykutty Aryankalayil, Radiation Oncology Branch, Center for Cancer Research, National Cancer Institute, 10 Center Drive, Room B3B406, Bethesda, MD 20892; email: aryankalayilm@mail.nih.gov.

labor-intensive protocol limits its application in mass screenings and demonstrates the need for more rapid, high-throughput methods. Recent developments of assays such as the protein-based Fluorescent Automated Screening Tool for Dosimetry (FAST-DOSE) and other blood-based proteomic, metabolomic, and transcriptomic signatures demonstrate improvements in biodosimetry methods (12–19).

Assays based on microRNA (miRNA) expression changes are of great interest due to their stability in room temperature biofluids and their regulatory roles in the radiation response (20–24). Recent work has demonstrated the potential for circulating miRNA expression profiles to identify radiation exposure (17, 25–29). However, individual molecules often exhibit varying expression levels across both dose and time after exposure and should therefore be approached with caution. Given the large regulatory network and abundance of interactions between miRNAs, long non-coding RNAs, and mRNAs, an integrated expression signature of blood based RNAs is likely to be more robust and shows potential for use in radiation biodosimetry (24, 30, 31).

Establishing an accurate, integrated RNA signature for biodosimetry will require an understanding of the factors that cause differences in radiation responses across the general population. Inherent to the radiation response is the ability to repair DNA damage, which could be affected by immune status, pre-existing conditions, and genetic background (32, 33). In mice, differences in radiosensitivity across strains are apparent both in LD50 variation across populations (34) and susceptibility of certain strains to specific clinical pathologies, including radiation-induced lung fibrosis or cancers (35, 36). Recent studies have addressed differences in circulating gene and protein expression between mice with varying DNA repair mechanisms and genetic backgrounds (36–39). Studies of differences in non-coding RNA expression have focused on whole-thorax irradiation (40), presenting a need to understand differences in response to whole body irradiation (WBI) across several strains of mice to employ the use of non-coding RNAs in biodosimetry.

In an effort towards our development of an integrated non-coding RNA signature for radiation biodosimetry, we have expanded our previous work with blood-based miRNA signatures from whole-body irradiated C57BL/6 mice by profiling miRNA expression changes in two additional strains, C3H/HeJ and BALB/c after whole-body exposure. We analyzed the global miRNA response to radiation in each of these strains and compared expression across all three strains to improve our understanding of how baseline and radiation-induced miRNA expression differs among a heterogeneous population. Our goal was to create a proof of concept that, despite the underlying heterogeneity of a population, blood-based biomarker panels could aid in tiering victims into categories. These categories would need to differentiate between people who received a potentially lethal dose and need immediate care (high risk, 8 Gy vs. 1 Gy,

2 Gy, 4 Gy) compared to patients who received a higher dose and need care (high dose, 4 Gy and 8 Gy vs. 1 Gy and 2 Gy), enabling clinicians to deliver care more efficiently in scarce-resources situations.

MATERIALS AND METHODS

Whole-Body Irradiation

Female C3H/HeJ and BALB/c mice from 8–14 weeks of age received whole-body exposure of 0 Gy (sham) or 1, 2, 4 or 8 Gy using a Precision X-ray Irradiator cabinet at a dose rate of 3.59 Gy/min. Animals were placed within plexiglass containers (with air holes) allowing freedom of movement. Irradiation was done with 2 animals per plexiglass container and the exposure was anterior/posterior (AP/PA). The beam geometry entirely encompassed the plexiglass container and previous dosimetry has validated beam uniformity within acceptable ranges and in-run dosimetry was not carried out. Dose rate was previously calibrated based on the procedures described in American Association of Physicist in Medicine Task Group Report 61 with regard to the following conditions: X-ray tube potential was 300 kV, half-value layer was 0.8 mm copper, source-to-surface distance was 50 cm. Dose rate was measured at 2 cm depth in solid water phantom using a PTW model N23342 ion chamber (Freiburg, Germany) and Inovision model 35040 electrometer (Chesterfield, MI). Three to four animals per dose per timepoint for each strain were included in this study.

Terminal Blood Collection from Mice using Cardiac Puncture

Blood samples were collected at 1, 2, 3, or 7 days postirradiation. Mice were anesthetized with 2.5–5.5% isoflurane and approximately 500 μ L of blood was drawn via cardiac puncture into RNA protect animal blood tubes (QIAGEN, Germantown, MD). Samples were inverted 8–10 times, incubated for 2 h at room temperature, and stored at -80°C .

RNA Isolation and Purification

Total RNA was isolated from whole blood using the RNeasy Animal Protect Blood Kit (QIAGEN). Briefly, blood cells were lysed in the RNA Protect Animal Blood Tubes to release and precipitate intracellular RNA. RNA and cellular debris were then pelleted and washed once with RNase-free water before performing isolation according to the manufacturer's protocol. Total RNA was further purified and concentrated using the Total RNA Purification Kit (Norgen Biotek Corp, Thorold, Canada). Quantity and purity of the RNA was assessed using a DS-11 Series Spectrophotometer/Fluorometer (DeNovix, Wilmington, DE).

NanoString nCounter miRNA Panel

NanoString nCounter Mouse v1.5 miRNA Panels (NanoString, Seattle, WA) were used to analyze blood-based miRNA expression. These panels include unique nCounter Capture and Reporter probe pairs for 578 well-characterized endogenous mouse miRNAs, 33 viral miRNAs, and four endogenous reference controls (*Actb*, *B2m*, *Gapdh* and *Rpl19*). Samples were prepared according to the manufacturer's protocol. Briefly, 100 ng of total RNA per sample was used to prepare miRNA via ligation of sequence-specific tags onto the 3' end of target miRNAs and subsequent purification to remove non-ligated tags. Samples were then hybridized to Reporter and Capture probes in an overnight reaction at 65°C , followed by purification to remove excess probes. Digital counts of miRNA sequences were performed by scanning each hybridized sample on the nCounter Digital Analyzer.

Statistical Analysis of miRNA Expression Profiles

The nSolver Analysis software (NanoString) was used to normalize raw miRNA counts and corrected for non-specific counts from the NanoString miRNA panels. Normalization included the following three steps: 1. Positive control normalization with respect to the geometric mean of the positive control targets in each panel; 2. CodeSet content normalization with respect to the geometric mean of the top 100 expressed miRNA targets; and 3. Background thresholding with respect to the geometric mean of the ligation negative controls. After normalization, probes with counts at or below the background level in all conditions were filtered out. For each miRNA probe that passed the background cutoff, counts were averaged across all samples and the standard deviation from this mean was calculated for each sample. A 50th percentile cutoff for both the mean and standard deviation was applied. Data were then analyzed using R environment for statistical computing (<https://www.R-project.org>) (41). Two-way analysis of variance (ANOVA) analysis was performed to identify main effects of dose and time as independent variables followed by false discovery rate (FDR) by Benjamini Hochberg method (42). miRNAs are deemed significant at $FDR \leq 0.05$. To evaluate pairwise dose response effect at each time point, one-way ANOVA followed by post hoc analysis by Dunnett's test was performed to compare multiple doses with control. Dose-specific differential expression patterns at each timepoint ($|FC| > 1.5$; adjusted $P \leq 0.05$) were selected for further analyses. A summary including the number of miRNAs that passed at each cut-off is given in Table 1.

Comparative Analysis of C3H/HeJ, BALB/c, and C57BL/6 miRNA Expression Profiles

Common doses and timepoints between the current study and our previous study (24) were selected [0 Gy, 2 Gy, 4 Gy, 8 Gy; 1, 2 and 7 days after whole-body irradiation (WBI)] and normalized miRNA data from each strain was subset accordingly. RNA from the prior study (C57BL/6 mice) was assayed as previously described (24). Raw data for C57BL/6 can be found in the Gene Expression Omnibus, an NCI repository (GSE107057). One-way ANOVA followed by Dunnett's test was performed separately for each strain to identify common differentially expressed miRNAs ($|FC| > 1.5$, $P < 0.05$) across all three strains in at least one dose and timepoint.

Pathway Enrichment Analysis of Experimentally Verified mRNA Targets of Common miRNAs

Radiation responsive miRNAs common to the three strains were used to determine Kyoto Encyclopedia of Genes and Genomes (KEGG) pathway enrichment using DIANA-miRPath v.3 (<http://diana.imis.athena-innovation.gr/DianaTools/>) (43). Significantly regulated pathways by Fisher's Exact Test were identified by $P < 0.05$.

Pooled Strain Prediction

To address if individual strains can be classified from pooled data and generate easy to visualize decision rules, we used predictive classification and regression trees (CART) (44) from Recursive Partitioning and Regression Trees (rpart) package in R. The algorithm of decision tree models works by repeatedly partitioning the data into multiple sub-spaces, so that the outcome in each final sub-space is as homogeneous as possible. This approach is technically called recursive partitioning. The produced result consists of a set of rules used for predicting the categorical variable, for classification trees, and the decision rules generated by the CART predictive model are visualized as a binary tree. Input to the model included pooled data from three strains for common doses (0 Gy, 2 Gy, 4 Gy and 8 Gy) and time points (1, 2 and 7 days). For each model we divided the data into train (70%) and test (30%) samples. We chose three criteria to test the

strain prediction for each time point selected: 1. irradiated vs. unirradiated; 2. high dose (4 Gy, 8 Gy) vs. low dose (1 Gy, 2 Gy); and 3. viable (1 Gy, 2 Gy, 4 Gy) vs. high risk (8 Gy). To include the 3 days after whole-body exposure timepoint that was missing in pooled sample data, we analyzed an additional model for day 3 using the two strain data available (C3H/HeJ and BALB/c strains only).

Validation of miRNA using qRT-PCR

Due to limited sample quantity, BALB/c validation was not possible. Validation of miR-150-5p and miR-23a was performed in 24h samples for C57BL/6 mice at 1 Gy, 2 Gy, 4 Gy, 8 Gy and sham irradiated. No 48 h samples were available for C57BL/6 mice. Validation of miR-150-5p and miR-23a-3p was done in 24 h and 48 h samples for C3H/HeJ mice at 1 Gy, 2 Gy, 4 Gy, 8 Gy and sham irradiated. For miR-92a-5p, miR-99a-5p and miR-223a-5p were performed in 48 h samples for C3H/HeJ mice at 1 Gy, 2 Gy, 4 Gy, 8 Gy and sham irradiated. Since 48 h and 72 h showed the highest differential expression between sham and irradiated animals, we chose this time for the C3H/HeJ mice. Three samples from each time and dose were used for qRT-PCR. Samples were validated using the miRCURY LNA RT Kit (Qiagen, Cat. No./ID 339340) for cDNA synthesis and miRCURY LNA SYBR Green PCR Kit (Qiagen, Cat. No./ID 339345) per manufacturer protocols. The following miRCURY LNA PCR primers were purchased from Qiagen (Cat. No./ID 339306): miR-16-5p, miR-23a-3p, miR-92a-5p, miR-99a-5p, and miR-223a-5p. Reactions were conducted in ABI QuantStudio and analyzed with miR-16-5p as a known endogenous control (45). Fold change was produced using this formula:

$$dCT_{miRNA_sampleA} = CT_{miRNA_sampleA} - CT_{miR-16-5p_sampleA}$$

$$ddCT_{miRNA_sampleA} = dCT_{miRNA_sampleA} - dCT_{miRNA_control\ sample}$$

$$\text{Fold change}_{miRNA_sampleA} = 2^{-ddCT_{miRNA_sampleA}}$$

RESULTS

Circulating miRNA Expression after Whole-Body Irradiation Differs between C3H/HeJ and BALB/c Mice

To understand changes in circulating miRNA expression after irradiation, NanoString nCounter panels were used to profile 578 well-characterized miRNAs in the blood of C3H/HeJ and BALB/c mice collected on days 0–7 after whole-body exposure to 1 Gy, 2 Gy, 4 Gy, 8 Gy or sham. Overall, the number of differentially expressed miRNAs in irradiated vs. control samples was higher in C3H/HeJ than in BALB/c mice (Fig. 1 and Supplementary Table S1³; <https://doi.org/10.1667/RADE-23-00007.1.S1>), indicating a potential difference in the sensitivity of the miRNA response to whole-body exposure between these two strains. Within this observation, the dose and time distributions of significant miRNAs were similar across both strains. Both strains exhibited increasing numbers of miRNAs with increasing dose and a peak in differential expression at day 2 after WBI, with 12, 22, 20 and 31 miRNAs in BALB/c and 11, 40, 82 and 92 miRNAs in

³ Editor's note. The online version of this article (DOI: <https://doi.org/10.1667/RADE-23-00007.1>) contains supplementary information that is available to all authorized users.

TABLE 1
Summary of Selection Criteria for Identification of Differentially Expressed, Blood-based miRNAs after Whole-Body Irradiation

Test performed	miRNA probes passed							
	C3H/HeJ				BALB/c			
QC passed:	306				301			
1. Probes below background filtered out								
2. Probes within 50th percentile of standard deviation selected								
Two-way ANOVA main effects (FDR < 0.05):								
Time	40				11			
Dose	57				13			
One-way ANOVA and Dunnett's test: Each dose vs. control at each time-point; P < 0.05	D1	D2	D3	D7	D1	D2	D3	D7
	38	121	95	20	17	40	58	25

Note. All miRNAs were subject to QC criteria followed by one- and two-way analysis of variance to identify differentially expressed miRNAs that change with respect to dose and time.

C3H/HeJ mice 2 days after WBI of 1 Gy, 2 Gy, 4 Gy and 8 Gy, respectively (Fig. 1A). C57BL/6 mice showed a peak in shared miRNAs that were differentially expression at day 2 after WBI with 51 miRNA showing altered regulation across all doses; however, 7-day samples showed the most changes in miRNA expression at each dose (2 Gy, 4 Gy, 8 Gy and 12 Gy) (46). The overlap of miRNAs commonly expressed in C3H/HeJ and BALB/c strains was highest in 4 and 8 Gy irradiated mice, regardless of time after exposure, and 2 and 3 days after WBI,

regardless of the dose (Fig. 1B and C). At other doses and timepoints, few miRNAs were significantly expressed in both C3H/HeJ and BALB/c mice. After 1 Gy, neither strain showed any differential expression after 7 days, with minimal change after 3 days suggesting a shorter timescale and faster return to baseline for miRNA expression after a low dose of radiation, regardless of strain. All three strains (BALB/c, C3H/HeJ and C57BL/6) showed some continued alterations in miRNA expression at 7 days in 4 and 8 Gy samples (Fig. 1) (46). PCA analysis of the miRNA expression data

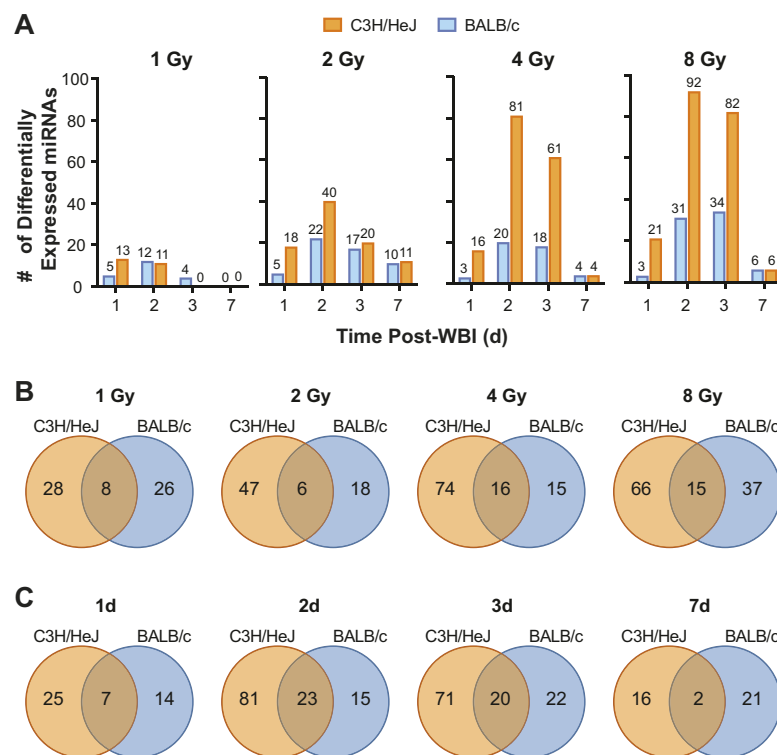


FIG. 1. Differential miRNA expression is most pronounced two days after WBI for C3H/HeJ and BALB/c mice. Panel A: For each strain, the number of differentially expressed miRNAs in irradiated samples vs. control samples was identified across all doses at each timepoint using one-way ANOVA. Overlap in expression between the two strains was determined for each (panel B) dose and (panel C) timepoint.

further highlights the similarities of expression patterns of 4 Gy and 8 Gy-exposed animals at days 2 and 3 after WBI, as these samples clustered together for both C3H/HeJ and BALB/c mice (Supplementary Fig. S1A and B; <https://doi.org/10.1667/RADE-23-00007.1.S2>). While the remaining C3H/HeJ samples formed a distinct cluster away from the 4 Gy and 8 Gy samples at days 2 and 3 after WBI, at day 7 postirradiation BALB/c mice that received 8 Gy of radiation also clustered with the two- and three-day samples, demonstrating a potentially more prolonged response from the higher doses in BALB/c mice.

Radiation-induced miRNA Expression is Regulated in a Time- and Dose-Dependent Manner

For each strain, we performed two-way ANOVA to understand the independent effects of dose and time on miRNA expression, selecting probes with a dose or time FDR <0.05. In C3H/HeJ and BALB/c strains, miRNA expression changed more in response to dose than to time, with 57 and 20 miRNAs having dose-dependent expression changes in C3H/HeJ and BALB/c mice, respectively (Fig. 2A and Supplementary Table S2; <https://doi.org/10.1667/RADE-23-00007.1.S3>). Both strains also had a relatively high overlap of miRNAs that showed both dose- and time-dependent changes (31 in C3H/HeJ and 7 in BALB/c), suggesting that while different dose exposures may be the primary factor driving miRNA regulation, the expression changes over time are also significant for many of these miRNAs. Additionally in both strains, 1 Gy and 2 Gy samples generally showed only slight increases or decreases in expression across all time points, while 4 Gy and 8 Gy samples had the most pronounced changes in expression magnitude (Fig. 2B and C). In C3H/HeJ samples, about half of the dose-dependent miRNAs showed a dose-responsive increase in relative expression, while the other half showed a dose-responsive decrease (Fig. 2B). Nearly all these miRNAs exhibited a peak in expression magnitude at days 2 and 3 after whole-body exposure, with similar patterns observed in the C3H/HeJ time-dependent miRNAs (Supplementary Fig. S2A; <https://doi.org/10.1667/RADE-23-00007.1.S4>). We saw a similar peak at day 2 after whole-body irradiation in our C57BL/6 data (46). In BALB/c samples, relative expression patterns in dose- and time-dependent miRNAs showed the highest relative expression in the control, followed by a decrease in expression over time (Fig. 2C and Supplementary Fig. S2B). This is evident by looking at the expression patterns over time of the top five dose-responsive miRNAs in BALB/c mice. Three miRNAs, miR-16, -142 and -1937a/b, exhibit detectable expression levels in 0 Gy samples but drop below detection limits at days 2 and 3 after WBI in 2, 4, and 8 Gy samples before increasing closer to baseline expression levels at day 7 (Supplementary Fig. S2C). In contrast, the top differentially expressed miRNAs in C3H/

HeJ mice exhibit a significant increase in response to irradiation at these timepoints before returning to baseline after 7 days (Supplementary Fig. S2D).

Differentially Expressed miRNAs Play Roles in Regulation of Metabolism and DNA Repair

To understand potential differences and similarities in function of the differentially expressed miRNAs in C3H/HeJ and BALB/c strains, we used DIANA-miRPath to identify gene targets of the miRNAs and their involvement in KEGG pathways. We found that the miRNAs in both strains regulate genes in 43 common pathways (Fig. 3A). Metabolic pathways such as fatty acid biosynthesis, fatty acid metabolism, and N-glycan biosynthesis were among some of the most significant pathways identified in both strains (Fig. 3B). These results highlight that while the expression of specific miRNAs differs between C3H/HeJ and BALB/c mice after WBI, both strains likely undergo dysregulation of similar pathways related to DEARE (4, 5).

We also sought to determine how alterations in miRNA may impact DNA repair after radiation injury. Prior data was used to choose miRNA of interest related to DNA repair and damage response (47, 48). Briefly, some miRNA including miR-34a, -100, -101, -193, -421, and -192, which have previously been associated with DNA repair did not show significant changes in expression in either mouse strain (data not shown). However, miR-16, -29a, -29b, -29c, -183, -210, -125-5p, -21, -194 -148a and -148b show differential expression after radiation injury in C3H/HeJ (Fig. 3C). In BALB/c mice the miRNAs miR-29c and -125a-5p had at least one sample at background expression levels for all doses and times (Fig. 3D). Notably, dysregulation of DNA repair-related miRNAs is largely resolved in C3H/HeJ mice by 7 days while downregulation of miRNAs seems to continue through this timepoint for BALB/c mice.

Comparative Analysis of Differential miRNA Expression in the Blood of C57BL/6, C3H/HeJ and BALB/c Mice

We previously used microarray analysis to identify changes in blood-based miRNA expression in C57BL/6 mice and identified a 23-miRNA signature that can distinguish irradiated from unirradiated mice (24). To understand similarities and differences in the miRNA expression profiles of C57BL/6, C3H/HeJ, and BALB/c mice, data from each strain were subset to include only 0 Gy, 2 Gy, 4 Gy, and 8 Gy doses at days 1, 2, and 7, which were the common conditions across all three strains. One-way ANOVA followed by Dunnett's test for each data subset from each strain yielded the significantly regulated miRNAs at these doses and timepoints. Comparison of the three separate ANOVA analyses revealed that 12 miRNAs were significantly regulated in at least one dose and timepoint in C3H/HeJ and BALB/c mice (Supplementary Fig. S4A; <https://doi.org/10.1667/RADE-23-00007.1.S5>), as well as C57BL/6 mice from our previous study (24). As

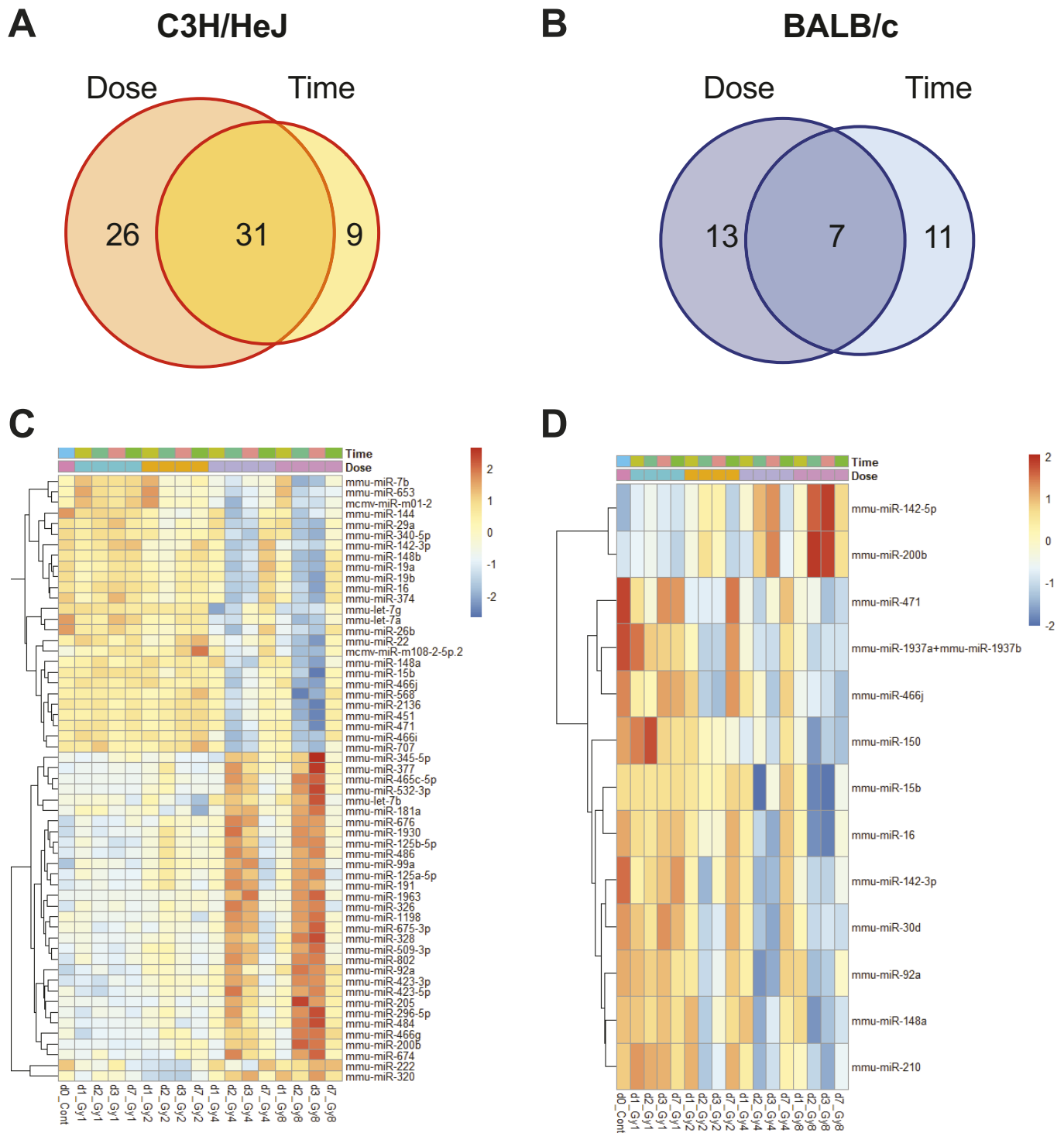


FIG. 2. Dose-dependent changes in blood-based miRNA expression are more significant than time-dependent changes after WBI. Panel A: Venn diagrams for C3H/HeJ and BALB/c strains display results of the two-way ANOVA that identified the number of miRNAs differentially expressed in dose- and time-dependent manners (FDR < 0.05). Panels B and C: Heatmaps and hierarchical clustering of miRNAs display relative expression of miRNAs that were most significantly regulated by changes in dose, independent of time, for (panel B) C3H/HeJ and (panel C) BALB/c mice. Color scales represent abundance of miRNAs after normalization with z-scoring across rows of the heatmap.

seen in the individual strain analyses, the most prominent expression changes occurred at day 2 postirradiation across all strains. By day 7 postirradiation, most expression levels returned to basal levels except for 8 Gy irradiated BALB/c

mice, which showed persistent downregulation of 8 of the miRNAs. Across all doses, no miRNAs were commonly expressed in all three strains at day 7. Notably, four miRNAs exhibited contrasting differential expression

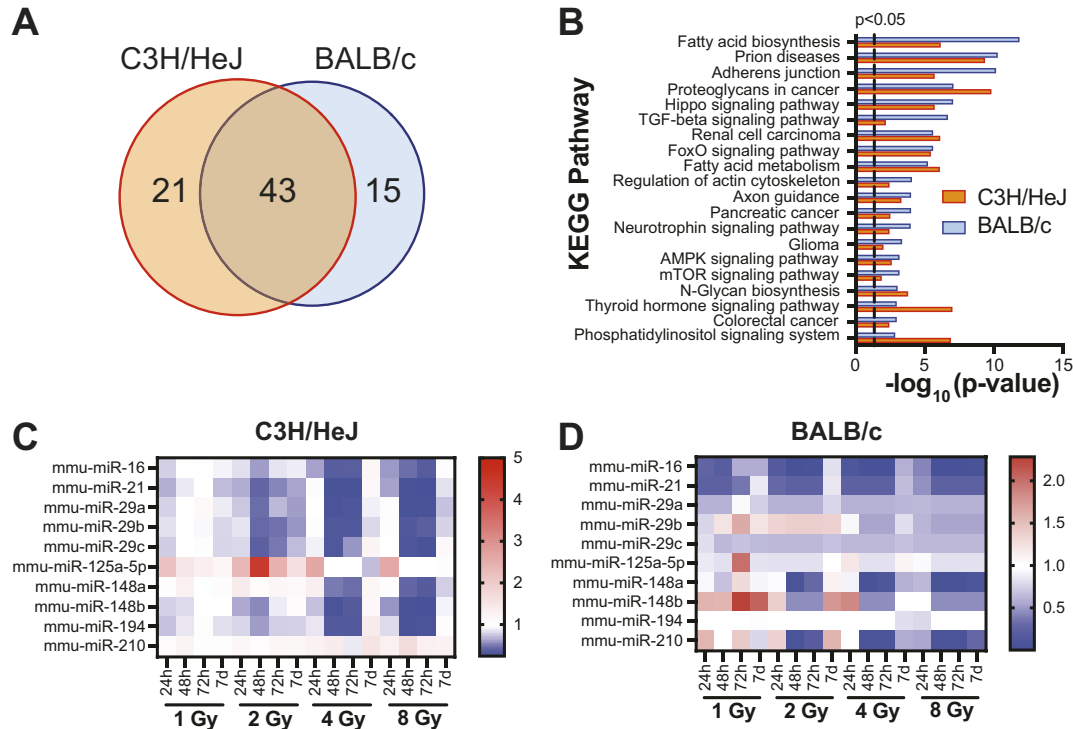


FIG. 3. Significantly regulated miRNAs play roles in similar pathways in C3H/HeJ and BALB/c mice. Panel A: Venn diagram displays overlap in pathway involvement between C3H/HeJ and BALB/c mice. DIANA-miRPath was used to identify pathway involvement of dose-dependent miRNAs in C3H/HeJ and BALB/c mice. Panel B: Pathways predicted to be most significant in both C3H/HeJ and BALB/c mice. Dashed line indicates P-value threshold ($P < 0.05$). Panels C and D: miRNAs related to DNA repair with at least one differentially expressed time point and dose are shown in heatmaps for (panel C) C3H/HeJ and (panel D) BALB/c mice. Data shows fold change of irradiated mice compared to 0 Gy controls indicated by color scale ($FC > 2$ or < 0.5 , $P < 0.05$).

patterns in BALB/c and C3H/HeJ. Of the four, miR-92a-3p, miR-223-3p, and miR-191-5p were upregulated in C3H/HeJ and C57BL/6 [Supplementary Fig. S4A (46)] but down regulated in BALB/c. The fourth miRNA, miR-20a-5p, was downregulated in BALB/c and C57BL/6 but upregulated in C3H/HeJ. Pathway analysis indicates these 12 miRNAs are involved in lysine degradation, the hippo signaling pathway and the insulin signaling pathway among others (Supplementary Fig. S4B). We sought to validate these Nanostring results through qRT-PCR. Due to limited quantities of RNA, we validated only C3H/HeJ samples at 48 h since this was the time point with the highest differential expression. As miR-150-5p has previously been identified as a useful radiation biomarker in prior studies, including our own, we sought to validate miR-150-5p in C3H/HeJ and C57BL/6. In Supplementary Fig. S4B we show decreased expression of miR-150-5p in C57BL/6 at 24 h as anticipated, in the 4 Gy and 8 Gy samples. We also see a significant decrease in miR-150-5p at 4 Gy but not 8 Gy in the 24 h C3H/HeJ samples but observed no significant changes in the C3H/HeJ samples at 48 h (Supplementary Fig. S4C and D), respectively. We chose several miRNA that we noted were differentially expressed in C3H/HeJ and Balb/C strains (Supplementary Fig. S3; <https://doi.org/10.1667/RADE-23-00007.1.S6>). These miRNA are shown in Supplementary Fig. S4D

(<https://doi.org/10.1667/RADE-23-00007.1.S5>) for qRT-PCR and Supplementary Fig. S4E for Nanostring. Fold change for qRT-PCR of select miRNA: miR-99a-5p, miR-92a-3p, miR-150-5p, miR-223-5p, and miR-466j comparing irradiated samples to control are shown with asterisks (*) to mark significant (fold change > 1.5 , $P < 0.05$) changes. Similar overall trends are observed between qRT-PCR and Nanostring samples for miR-99a-5p, miR-92a-3p, miR-150-5p and miR-223-5p. However, for miR-466j we observed downregulation in the Nanostring results and upregulation in the qRT-PCR. We observed tighter expression changes between samples for qRT-PCR compared to Nanostring.

Pooled miRNA Expression Data Enables Decision Tree Model that Distinguishes Irradiated from Unirradiated Subjects with High Accuracy

Our goal is to develop a robust RNA signature to be used for radiation biodosimetry. We therefore sought to determine whether we could identify a set of miRNAs that could differentiate exposed from unexposed mice, independent of strain, with the secondary goal of parsing out mice that received low (1 Gy, 2 Gy) from high doses (4 Gy, 8 Gy) and those that would be deemed viable (1 Gy, 2 Gy, 4 Gy) from those at high risk (8 Gy) after exposure. We pooled the expression data of all three strains and used

recursive partitioning to develop a tree model consisting of multiple miRNAs at each timepoint that could determine radiation exposure and risk levels of mice. Our tree models, a supervised learning algorithm, were designed to use miRNAs to differentiate between two categories, e.g., radiation or no radiation. In the context of this model, an important variable or feature is any miRNA that was selected to split during the tree building process, and how much the squared error (over all trees) improved (decreased) as a result. In the end we kept the miRNAs selected by the model that are relevant for the classification. Samples were pooled and then tested to differentiate radiation vs. no radiation or other categories. As such, C3H/HeJ, C57BL/6, and BALB/c mice that received radiation were combined. Overall, samples from irradiated groups showed similar trends, allowing the decision tree to categorize them with high accuracy, despite strain heterogeneity. Notably, while the expression patterns of many of the individual miRNAs from pooled samples did not show significant differences between irradiated and control samples (Fig. 4), a combination of miRNAs predicted exposed from unexposed mice with 100% accuracy at days 1 and 2 after WBI (Table 2). Figure 4A shows those most important for predicting exposed vs. unexposed, Fig. 4B showing those most important for distinguishing low vs. high dose, and Fig. 4C showing the most important miRNAs for predicting viable vs. high-risk exposure.

Differences between strains and their expression of miRNAs was notable, however, this did not prevent us from developing statistically significant predictions. At day 1, miR-19a, miR-16, and let-7f were the most important miRNA for developing a tree model to predict exposed vs. unexposed across all strains (Table 2). By day 2, miR-326, miR-148a and let-7a were most important. By day 7, statistical significance could not be reached and a set of miRNAs from our data could not reliably predict which mice had been exposed to radiation. Our miRNA signatures were also less reliable when predicting more specific populations beyond exposed and unexposed. At day 1 our test miRNA cluster showed a 66% accuracy in differentiating between animals receiving high and low doses with miRNAs let-7a, let-7e, miR-130b, miR-132, miR-19a, miR-222 and miR-301a being most important for this signature. As expected, based upon our initial tree model for predicting exposed from unexposed subjects, the day 7 miRNA expression data failed to reliably predict differences between high and low doses of radiation and viable and high-risk subjects. Prediction of high-risk dose exposure could only be assessed at day 1 postirradiation ($P < 0.0082$), with miRNAs let-7a, let-7d, miR-1224, miR-19a, miR-320, and miR-328 being most important for developing this prediction.

We next sought to determine if the three day postirradiation timepoint would be useful in developing predictions, as this was a timepoint with peak expression of many miRNAs in BALB/c and C3H/HeJ mice (Fig. 1). To do this, we used only our BALB/c and C3H/HeJ data to

develop prediction trees at days 1, 2, 3, and 7 postirradiation, still focusing on exposed vs. unexposed, low dose vs. high dose, and viable vs. high-risk exposure (Supplementary Table S3; <https://doi.org/10.1667/RADE-23-00007.1.S7>). Interestingly, removing the C57BL/6 mouse data led to decreased accuracy and non-significant P values for our exposed vs. unexposed markers, with the pooled data decision tree showing $P = 0.0625$ on days 1 and 2. The two-strain prediction at day 2 for low dose vs. high dose was more accurate and had a lower P value than the day 2 prediction with 3 strains. Both the 2- and 3-strain prediction models used miR-15b and let-7a (Table 2 and Supplementary Table S3). Interestingly, when only C3H/HeJ and BALB/c mice were used for prediction miR-374 became important in both predicting exposed vs. unexposed, low dose vs. high dose, and viable vs. high risk. This miRNA regulates cell growth and differentiation in normal tissue through multiple mRNA targets involved in the PI3K/AKT pathway (49).

Finally, we wanted to understand how the miRNAs in our prediction signatures may be relevant to biological pathways and processes, giving potential insight into the biological mechanisms of the miRNA response to radiation across the pooled population. We performed pathway analysis using the miRNAs most important to the prediction signatures that defined exposed vs. unexposed (Fig. 5A), high- vs. low-dose irradiation (Fig. 5B), and high-risk vs. viable subjects (Fig. 5C). Notably, lysine degradation, fatty acid metabolism, and proteoglycans in cancer are shown across different categories and times. This suggests that while the same miRNAs are not always dysregulated at all time points, the impact of radiation on pathway regulation remains consistent.

DISCUSSION

Early identification of radiation exposure after a nuclear disaster is crucial for efficient allocation of resources and may enable mitigation of DEARE. While mouse models are widely used to develop assays for radiation biodosimetry, it is well established that proteomic, genomic, and metabolomic responses to radiation can vary greatly across genetic backgrounds and strains.

Based on our previously published miRNA signature identified in the blood of C57BL/6 mice, we sought to understand how circulating miRNA expression differs across other commonly used mouse strains, radioresistant C57BL/6J and C3H/HeJ, and radiosensitive BALB/c, and whether common miRNAs could successfully sort irradiated from unirradiated subjects to aid in development of a robust signature for radiation biodosimetry. Our previous work with C57BL/6 mice found that blood-based miRNA expression changes are most significant at day 2 after WBI, with very few miRNAs maintaining differential expression after 7 days (24). The present study confirms this pattern in both C3H/HeJ and BALB/c mice, and expands upon the

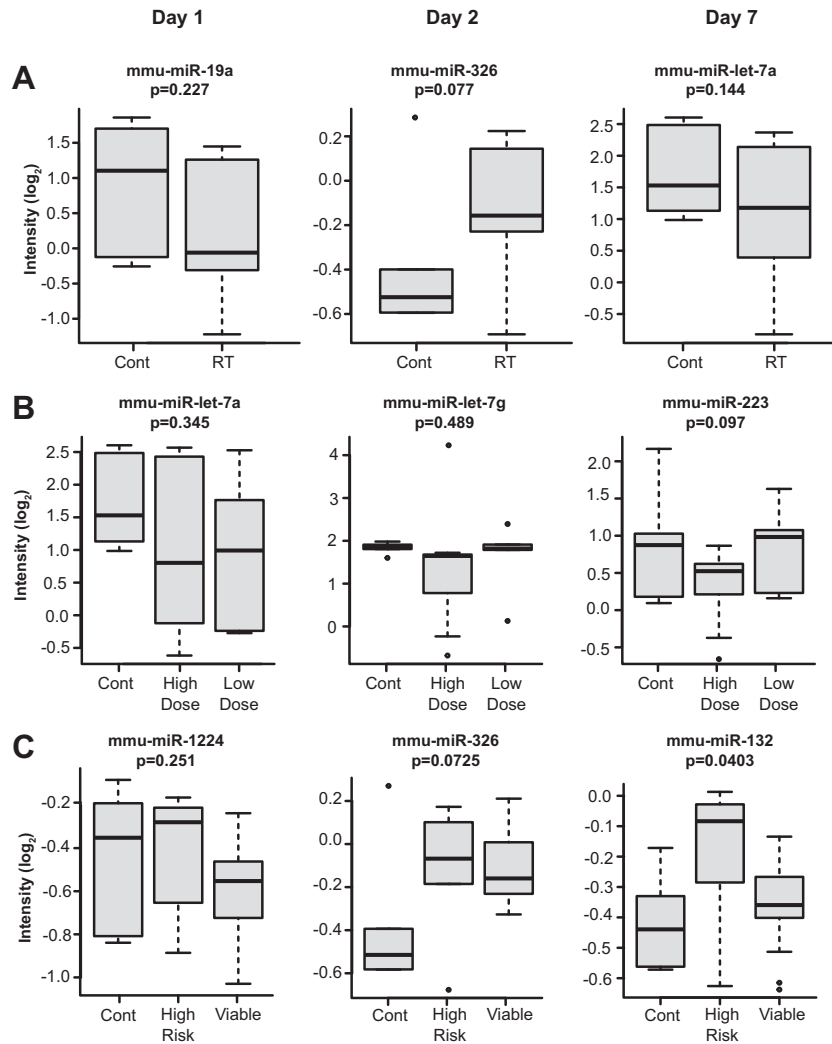


FIG. 4. Differential expression of individual miRNAs important for prediction signatures show no significant differences between irradiated and unirradiated mice. Box plots show mean expression of the most important miRNA across all strains at days 1, 2, and 7 after WBI in each prediction model: (panel A) irradiated (RT) and unirradiated (Cont) mice; (panel B) Cont, high dose (4 and 8 Gy), and low dose (2 Gy); and (panel C) Cont, high risk (8 Gy), and viable (2 and 4 Gy) mice.

time course by showing a similar number of differentially expressed miRNAs in both strains at day 3 after WBI compared to two days. Additionally, we confirmed the dose-responsive nature of miRNAs across these strains, with more frequent and prolonged expression changes at higher doses such as 4 Gy and 8 Gy. Interestingly, the expression of specific miRNAs varied greatly across strains, with relatively few miRNAs commonly expressed in the blood of all three strains in at least one condition. It is evident that there is substantial variability in the expression of specific miRNAs when comparing these three strains. Notably, while we saw a decrease in miR-150-5p, a lymphocyte marker and negative regulator of inflammation, after 4 Gy and 8 Gy doses in C57BL/6 samples at 24 h, we did not see a decrease in expression in our C3H/HeJ samples at 48 h. In the sub-strain C3Hf/Sed/Kam, researchers required 13.92 Gy whole-thorax exposure

to decrease the expression of miR-150-5p by day 2 (50). This may be related to the impaired immune system of C3H/HeJ mice who are *Lps^{mut}*, TLR4 deficient (51). It highlights the importance of using multiple biomarkers to establish both dose and triage methods in a heterogeneous population that may include the immune compromised.

Prior research has shown that the more radiosensitive BALB/c strain exhibits higher expression of γ -H2AX and greater numbers of micronuclei in skin tissue at day 7 after 10 Gy WBI compared to C3H/HeJ and C57BL/6 mice (52). Similarly, γ -H2AX foci showed slower DNA repair kinetics in ex vivo lymphocytes after irradiation in BALB/c compared to C57BL/6 mice; this is attributed to mutations in the DNA-PKcs enzyme in the non-homologous end-joining (NHEJ) pathway of BALB/c mice (53, 54).

We also observed differences in expression of DNA repair-related miRNAs between the BALB/c mice and

TABLE 2
Three-strain Tree Model Summary

Model	Time after WBI	Test data accuracy (95% CI)	P	Important miRNAs by tree model (score)
Exposed vs. unexposed	Day 1	1 (0.5407, 1)	0.015	mmu-miR-19a (100), mmu-miR-16 (78.59), mmu-miR-let-7f (69.08)
	Day 2	1 (0.5407, 1)	0.015	mmu-miR-326 (93.96), mmu-miR-148a (54.562), mmu-miR-let-7a (23.189)
	Day 7	0.66 (0.2228, 0.9567)	0.34	mmu-miR-let-7a (100), mmu-miR-16 (73.53), mmu-miR-99a (59.88)
Low dose vs. high dose	Day 1	0.66 (0.2993, 0.9251)	0.042	mmu-let-7a (100), mmu-let-7e (85.50), mmu-miR-130b (26.40), mmu-miR-132 (30.59), mmu-miR-19a (32.96), mmu-miR-222 (97.61), mmu-miR-301a (36.47)
	Day 2	0.66 (0.2993, 0.9251)	0.042	mmu-let-7a (41.273), mmu-let-7g (100), mmu-miR-15b (80.90), mmu-miR-326 (43.94)
	Day 7	0.33 (0.0749, 0.7007)	0.62	mmu-let-7a (65.76), mmu-miR-1224 (22.16), mmu-miR-223 (94.25), mmu-miR-29c (44.042)
Viable vs. high risk	Day 1	0.777 (0.3999, 0.9719)	0.0082	mmu-let-7a (33.66), mmu-let-7d (24.73), mmu-miR-1224 (69.40), mmu-miR-19a (42.13), mmu-miR-320 (10.61), mmu-miR-328 (62.65)
	Day 2	0.444 (0.137, 0.788)	0.35	mmu-let-7a (37.30), mmu-let-7f (24.80), mmu-miR-130b (31.32), mmu-miR-326 (88.84), mmu-miR-484 (29.83)
	Day 7	0.333 (0.0749, 0.7007)	0.62	mmu-let-7a (45.73), mmu-miR-132 (100), mmu-miR-148a (39.65), mmu-miR-200c (7.456), mmu-miR-223 (35.94), mmu-miR-322 (71.73)

Note. Tree model summary. Table showing time, prediction purpose (exposed vs. unexposed, high dose vs. low dose, or high risk), accuracy and 95% confidence interval, P value, and most important miRNAs used to develop the prediction across 3 mouse strains (C3H/HeJ, BALB/c and C57BL/6).

C3H/HeJ mice. Notably, multiple miRNAs remained downregulated at day 7 after 8 Gy irradiation in BALB/c, whereas C3H/HeJ mice showed a return to baseline expression by this timepoint. While miR-148a, -148b, -183, -210, and let-7a are negatively associated with homologous recombination and their upregulation leads to downregulation of DNA-repair genes *BRCA1/2*, *RAD50*, and *RAD51* [55]. This is an interesting result considering we see upregulation of several of these miRNAs in BALB/c samples. While the NHEJ pathway has previously been considered inefficient in BALB/c mice due to the DNA-PKcs mutation, no studies have previously highlighted potential disruption of homologous repair in these mice after radiation injury.

Several key miRNAs identified in our study have also been implicated in other pathways. Namely, miR-29 family members regulate fibrinogen, and their downregulation is associated with fibrosis in the liver and end stage heart failure (56), which are chronic effects of radiation. Interestingly, miR-148a/b-3p is downregulated in endothelial cells compared to umbilical cord cells, and this downregulation is necessary for endothelial cell differentiation and increased angiogenesis through NRPI and VEGF, respectively (57). Downregulation of miR-210 is also associated with endothelial cell dysfunction and reactive oxygen species upregulation in rat aorta (58). Taken together, the observed downregulation of these miRNAs in our data could potentially be early indicators of long-term response to radiation, though further investigation is needed.

While an overall return to baseline expression was observed for most miRNAs in the blood of C3H/HeJ mice

by day 7, BALB/c mice continued to show many altered miRNA at day 7 postirradiation in 4 and 8 Gy samples (data not shown). We acknowledge that miRNA in the tissues of these mice may still be dysregulated as prior reports have shown, and that C3H mice are known to develop lung fibrosis months after irradiation, which is undoubtedly due to continued changes in RNA after irradiation. Our data does not conflict with other reports, rather we highlight differences in our mouse strains' responses to radiation injury. The animal model chosen for radiation injury will impact RNA response. Our goal was to show that despite these strain- or species-specific changes, we could still find universal miRNA markers that could be seen across groups as a method to mirror human heterogeneity.

KEGG pathway analysis was performed to understand the predicted functions of miRNAs relevant to predicting general radiation exposure, high-dose exposure, and high-risk exposure. Interestingly, the fatty acid metabolism, fatty acid biosynthesis, and fatty acid degradation pathways are dysregulated in all strains within predicted miRNAs in at least one time point. Interestingly, non-human primates showed changes in diacylglycerol and triacylglycerol composition in blood 7 days after WBI (2, 4, 6, 7 and 10 Gy) which was previously linked to inflammation and apoptosis (59). The impact of anticipated alterations in lysine degradation according to changes in miRNA require further study; however, prior research has indicated that high levels of lysine taken orally are correlated with improved healing of oral mucositis in patients after radiation exposure, can protect kidney structures from damage due to hypertension, and can regulate fatty acid

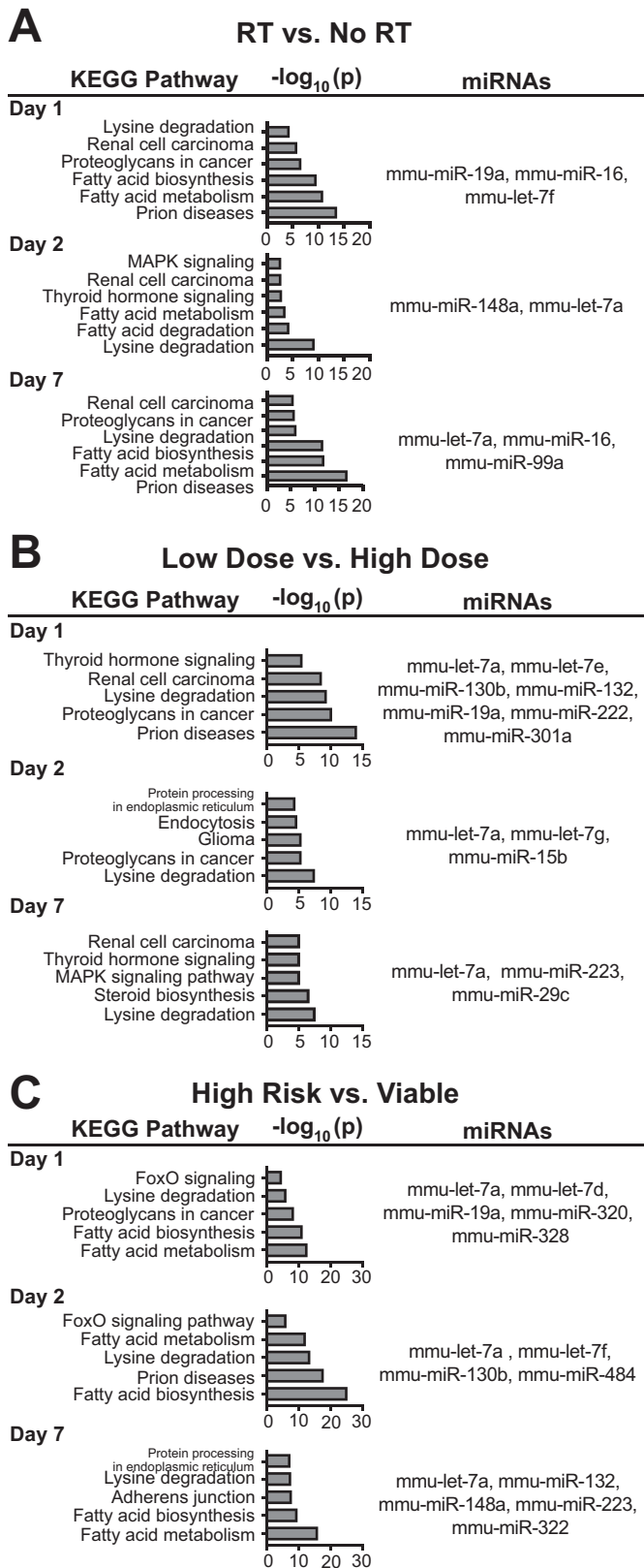


FIG. 5. Pathway analysis of miRNAs important for predictive signatures. DIANA tools miR-path was used to predict pathway regulation by the miRNAs most important to signatures that predict (panel A) irradiated (RT) vs. unirradiated (Cont), (panel B) high vs. low dose, and (panel C) high risk vs. viable subjects. Pathway names, $-\log_{10}(p)$, and miRNA in pathway are shown for each set of miRNAs.

synthesis through formation of chemical conjugates with malonyl-CoA (60, 61). Because miRNAs are known to have multiple gene targets based on various factors such as tissue type and species, future mechanistic studies to understand how these miRNAs regulate the identified KEGG pathways and DNA repair must be undertaken.

In addition to involvement in KEGG pathways, several of the common miRNAs identified in C3H/HeJ and BALB/c alone have been reported for their involvement in radiosensitization and general response to radiation. Specifically, miR-20a may promote radioresistance by targeting Notch signaling via NPAS2, which regulates apoptosis, cell cycle, and DNA damage response pathways (62). Both miR-19a and miR-142-5p are associated with regulation of inflammatory pathways and were differentially expressed in rat blood at two weeks after 15 Gy whole-thorax irradiation (63, 64). Additionally, miR-142-5p has been shown to increase expression of profibrotic genes and M2 macrophage polarization to promote murine lung fibrosis (65), which is a major concern in terms of the chronic effects of radiation exposure.

Specific expression data may not directly contribute to our development of a universal test to determine the objective dose of exposure. However, these miRNA biomarkers may be useful in creating a medical triage decision tree. For example, in the more radiosensitive BALB/c mice, miR-210 dropped close to background levels through day 7 after 8 Gy WBI, while C3H/HeJ mice showed no significant change in expression of this miRNA. Significant, prolonged downregulation like this could be an indication that the BALB/c mouse will not survive without intervention, and therefore warrants further investigation into its utility as a biomarker. Furthermore, these discrepancies in miRNA expression between the sensitive and resistant strains have potential to predict who is more likely to require urgent care versus routine follow-up. Further, differences in relative resistance as determined by reported LD50/30 for each strain may explain the difficulty in differentiating miRNAs altered at 1 Gy, 2 Gy, 4 Gy (viable) vs. 8 Gy (high risk) but allow for differentiation between low dose (1 and 2 Gy) compared to high dose (4 Gy and 8 Gy) (66–69). After a 4 Gy dose, BALB/c mice may already be succumbing to radiation injury, while C3H/HeJ and C57BL/6 are surviving.

We aimed to understand variation in radiation-induced miRNA expression across a genetically heterogeneous population by comparing expression profiles of C3H/HeJ, BALB/c, and C57BL/6 mice. Our study demonstrated that even across these diverse strains, we were able to predict with high accuracy exposed vs. unexposed mice at one and two days postirradiation. This highlights that early analysis is key to discerning irradiated subjects and that waiting until 7 days after exposure may be too late to accurately predict results, underscoring the time-sensitivity of miRNAs.

There has been recent interest in identifying extracellular miRNA that can be used as bio-markers for disease. While a non-invasive procedure would be preferable for a patient, miRNA in blood are typically of low abundance.

Development of clinically useful miRNA profiling platforms for accurate diagnosis requires that variability across samples due to batch effect, pre-processing, and normalization methods, be reduced to a minimum. Prior studies of different miRNA profiling platforms have been performed to discern which techniques are most useful (70, 71). Unlike RT-PCR or RNAseq, Nanostring does not use reverse transcription or amplification, which produces an exponential phase data points (72). Nanostring relies on capture probes that bind to target RNA and a reporter probe which acts as a molecular barcode (73). A scanner then counts each individual molecule. In one study looking at genes relevant to interferonopathy, Nanostring and qRT-PCR results showed a high correlation $R^2 = 0.87$, though some genes showed opposing differential regulation between these platforms (74). Our results, and those of others indicates that Nanostring may be a useful “first pass” tool for biomarker discovery, to be followed with validation through qRT-PCR.

While this study improves upon previous research of miRNA expression by comparing three strains of mice, our study is not without limitations. The conclusions we can draw about heterogeneity of radiation response across genetic backgrounds is limited by the selected strains of mice we used. Future murine studies should expand this number to include both males and females of inbred (e.g., CD2F1), and outbred strains (e.g., CD-1), due to their reported differences in radiation sensitivity (75). Additionally, while C3H/HeJ, BALB/c, and C57BL/6 have been reported to exhibit differences in their DNA repair pathways, immune response, protein synthesis rates, and hemostatic conditions (76–79), studying the effect of each of these factors individually on the miRNA expression could greatly improve our understanding of the RNA response to radiation. Furthermore, although they are beneficial for initial studies, mouse models are inherently limited by their limited translatability to humans. Future studies for identification and validation of biomarker signatures should be conducted in higher-order animal models like minipigs or non-human primates, which possess more genetic diversity and more closely recapitulate certain aspects of the human response to radiation. Additionally, the miRNA panels used to identify expression in the C3H/HeJ and BALB/c mice profiled 578 miRNAs compared to over 3,000 profiled in our previous C57BL/6 study. While the 578 miRNAs were the most characterized, it is possible that the low overlap of common miRNAs and significant predictive features across all three strains was limited by this difference and therefore a larger screen should be performed.

CONCLUSION

This study provides evidence that exposure to radiation does not elicit a uniform response across C3H/HeJ, BALB/c, and C57BL/6 mice, underscoring the need to consider variations in genetic background in the devel-

opment of radiation biodosimetry signatures. These signatures must be readily available, accurate, and time specific. In a mass casualty scenario, health care systems ideally should be able to test many people within 48 h, but dire situations could result in testing delays for some victims, necessitating an understanding of biomarkers at later timepoints. While variable across strains, the identification of differentially expressed miRNAs across all strains demonstrate the utility of using miRNAs as a biomarker for radiation exposure. In spite of this genetic heterogeneity in our subjects, we developed highly accurate miRNA signatures capable of predicting exposed and unexposed individuals as soon as 24 h after WBI. To improve efficacy of miRNA biomarkers, the complex regulatory network of coding and non-coding RNAs can be exploited to develop an integrated biomarker signature. Follow up experiments to confirm miRNA, long non-coding RNA, and mRNA expression profiles in additional strains of mice and higher-order animals will aid in this development. Ultimately, the identification of radiation-induced RNA expression changes will contribute to a decision tree that will enable segregation of exposed from unexposed victims of a radiobiological disaster.

SUPPLEMENTARY MATERIALS

Original data is included as Supplementary file (<https://doi.org/10.1667/RADE-23-00007.1.S8>), which contained miRNA data for C3H/HeJ and BALB/c mice. C57BL/6 data has previously been published.

Supplementary Table S1: miRNA lists from one-way ANOVA. Results of one-way ANOVA analyses performed for BALB/c and C3H/HeJ at each timepoint, including P values and fold changes for each dose.

Supplementary Table S2: miRNA lists from two-way ANOVA. Results of two-way ANOVA analyses performed for BALB/c and C3H/HeJ with respect to dose and to time, including FDR values for each miRNA.

Supplementary Table S3: Tree model summary for two-strain analysis. Table showing time, prediction purpose (exposed vs. unexposed, high dose vs. low dose, or high risk), accuracy and 95% confidence interval, P value, and most important miRNAs used to develop the prediction across 2 mouse strains (C3H/HeJ and BALB/c).

Supplementary Fig. S1: Principal component analysis of C3H/HeJ and BALB/c samples across dose and time. Principal component analysis of normalized miRNAs expressed in (panel A) C3H/HeJ and (panel B) BALB/c mice exposed to 0, 1, 2, 4, and 8 Gy at 1, 2, 3, and 7 days after WBI.

Supplementary Fig. S2: Two-way ANOVA results. Panels A and B: Heatmaps and hierarchical clustering of miRNAs display relative expression of miRNAs that were most significantly regulated by changes in time, independent of dose for (panel A) C3H/HeJ and (panel B) BALB/c strains. Color scale represents abundance of miRNAs after normalization with z-scoring across rows of heatmap.

Panels C and D: Bar plots show expression of the top 5 dose-dependent differentially expressed miRNAs over time for (panel C) BALB/c and (panel D) C3H/HeJ mice.

Supplementary Fig. S3: Twelve miRNAs are commonly differentially expressed in the blood of C3H/HeJ, BALB/c, and C57BL/6 mice after WBI. Panel A: miRNA expression data from common conditions between the C3H/HeJ and BALB/c datasets, as well as our previous C57BL/6 dataset, were compared to identify differences in miRNA expression across strains after WBI (2, 4 and 8 Gy; 1, 2 and 7 days). Plots display normalized NanoString counts from C3H/HeJ and BALB/c blood at each dose and timepoint. Data for C57BL/6 was previously published (24). Panel B: Pathway analysis was performed with DIANA-miRPath v.3 using the experimentally verified mRNA targets of the common differentially expressed miRNAs across all three strains of mice identified in panel A. Blue line indicates P value threshold ($P < 0.05$).

Supplementary Fig. S4: qRT-PCR validation of miRNA and Nanostring counts. CT values for miR-23a are presented for C57BL/6 and C3H/HeJ mice at 24 h to establish it as a useful endogenous control (panel A). In 24 h C57BL/6 mouse samples, miR-150-5p was validated by qRT-PCR expression analysis and shown to decrease after radiation injury at 4 Gy and 8 Gy (panel B). In 24h C3H/HeJ samples miR-150-5p was shown to decrease significantly at 4 Gy but not 8 Gy (panel C). We performed qRT-PCR using 48h C3H/HeJ samples for miR-92a-5p, miR-223-5p, miR-150-5p, miR-466j and miR-99a-5p (panel D) and compared it to Nanostring results (panel E). For qRT-PCR, a student's t-test was performed, asterisks (*) indicate all doses with significant fold change (fold change > 1.5 , $P < 0.05$) compared to 0 Gy.

ACKNOWLEDGMENTS

All animal studies were conducted in accordance with the principles and procedures outlined in the NIH Guide for the Care and Use of Animals and procedures were approved by the NIH Lab Animal Safety Program under an approved protocol. All mouse experiments were performed at the Radiation Oncology Branch of the National Cancer Institute, National Institutes of Health (Bethesda, MD). This study was supported by the NIH Intramural Research Program, National Cancer Institute, Center for Cancer Research and was supported by funding from the Radiation and Nuclear Countermeasures Program by NIAID (IAA #NRC-13028 and # Y2-OD-0332-01). The authors would like to acknowledge Dr. Eric Bernhard for critical comments on the manuscript.

Received: January 20, 2023; accepted: June 19, 2023; published online: August 1, 2023

REFERENCES

1. Macvittie TJ, Farese AM, Kane MA, ARS, DEARE, and Multiple-organ Injury: A Strategic and Tactical Approach to Link Radiation Effects, Animal Models, Medical Countermeasures, and Biomarker Development to Predict Clinical Outcome. *Health Phys* 2019; 116:453. doi:10.1097/HP.0000000000001050
2. Macvittie TJ, Farese AM. Defining the concomitant multiple organ injury within the ARS and DEARE in an animal model

- research platform. *Health Phys* 2020; 119:519–26. doi:10.1097/HP.0000000000001327
3. López M, Martín M. Medical management of the acute radiation syndrome. *Reports of Practical Oncology and Radiotherapy* 2011; 16:138. doi:10.1016/J.RPOR.2011.05.001
4. Unthank JL, Ortiz M, Trivedi H, et al. Cardiac and Renal Delayed Effects of Acute Radiation Exposure: Organ Differences in Vasculopathy, Inflammation, Senescence and Oxidative Balance. *Radiat Res* 2019; 191:383–97. doi:10.1667/RR15130.1
5. Micewicz ED, Iwamoto KS, Ratikan JA, et al. The Aftermath of Surviving Acute Radiation Hematopoietic Syndrome and its Mitigation. *Radiat Res* 2019; 191:323. doi:10.1667/rr15231.1
6. Coleman CN, Cliffer KD, DiCarlo AL, et al. Preparedness for a 'no-notice' mass-casualty incident: a nuclear detonation scenario. *Int J Radiat Biol* 2021; :1–5. doi:10.1080/09553002.2021.2013573
7. Coleman C, Koerner JF. Biodosimetry: Medicine, science, and systems to support the medical decision-maker following a large scale nuclear or radiation incident. *Radiat Prot Dosimetry* 2016; 172:38–46. doi:10.1093/rpd/ncw155
8. Sullivan JM, Prasanna PGS, Grace MB, et al. Assessment of Biodosimetry Methods for a Mass-Casualty Radiological Incident: Medical Response and Management Considerations. *Health Phys* 2013; 105:1–27. doi:10.1097/HP.0b013e31829cf221
9. Lloyd DC, Edwards AA, Moquet JE, et al. The role of cytogenetics in early triage of radiation casualties. In: *Applied Radiation and Isotopes*. 2000. 1107–12. doi:10.1016/S0969-8043(00)00054-3
10. Prasanna PGS, Moroni M, Pellmar TC. Triage dose assessment for partial-body exposure: Dicentric analysis. *Health Phys* 2010; 98:244–51. doi:10.1097/01.HP.0000348020.14969.4
11. Blumenthal DJ, Sugarman SL, Christensen DM, et al. Role of Dicentric Analysis in an Overarching Biodosimetry Strategy for Use Following a Nuclear Detonation in An Urban Environment. *Health Phys* 2014; 106:516–22. doi:10.1097/HP.0b013e3182a5f94f
12. Wang Q, Lee Y, Shuryak I, et al. Development of the FAST-DOSE assay system for high-throughput biodosimetry and radiation triage. *Sci Rep* 2020; 10:1–11. doi:10.1038/s41598-020-69460-7
13. Dressman HK, Muramoto GG, Chao NJ, et al. Gene expression signatures that predict radiation exposure in mice and humans. *PLoS Med* 2007; 4:690–701. doi:10.1371/journal.pmed.0040106
14. Lacombe J, Sima C, Amundson SA, et al. Candidate gene biodosimetry markers of exposure to external ionizing radiation in human blood: A systematic review. *PLoS One*. 2018; 13. doi:10.1371/journal.pone.0198851
15. Cruz-Garcia L, O'Brien G, Sipos B, et al. Generation of a Transcriptional Radiation Exposure Signature in Human Blood Using Long-Read Nanopore Sequencing. *Radiat Res* 2020; 193:143–54. doi:10.1667/RR15476.1
16. Paul S, Kleiman NJ, Amundson SA. Transcriptomic responses in mouse blood during the first week after in vivo gamma irradiation. *Sci Rep* 2019; 9. doi:10.1038/s41598-019-54780-0
17. Jacob NK, Cooley J V., Yee TN, et al. Identification of Sensitive Serum microRNA Biomarkers for Radiation Biodosimetry. *PLoS One* 2013; 8. doi:10.1371/journal.pone.0057603
18. Sproull M, Kramp T, Tandle A, et al. Multivariate Analysis of Radiation Responsive Proteins to Predict Radiation Exposure in Total-Body Irradiation and Partial-Body Irradiation Models. *Radiat Res* 2017; 187:251–8. doi:10.1667/RR14558.1
19. Golla S, Golla JP, Krausz KW, et al. Metabolomic Analysis of Mice Exposed to Gamma Radiation Reveals a Systemic Understanding of Total-Body Exposure. *Radiat Res* 2017; 187:612–29. doi:10.1667/RR14592.1
20. Palayoor ST, John-Aryankalayil M, Makinde AY, et al. Differential Expression of Stress and Immune Response Pathway

- Transcripts and miRNAs in Normal Human Endothelial Cells Subjected to Fractionated or Single-Dose Radiation. *Mol Cancer Res* 2014; 12:1002–15. doi:10.1158/1541-7786.MCR-13-0623.
21. Thapar R. Regulation of DNA double-strand break repair by non-coding RNAs. *Molecules*. 2018; 23. doi:10.3390/molecules23112789
 22. Scott E, Loya K, Mountford J, et al. MicroRNA regulation of endothelial homeostasis and commitment - Implications for vascular regeneration strategies using stem cell therapies. *Free Radic Biol Med*. 2013; 64:52–60. doi:10.1016/j.freeradbiomed.2013.04.037
 23. He Y, Jing Y, Wei F, et al. Long non-coding RNA PVT1 predicts poor prognosis and induces radioresistance by regulating DNA repair and cell apoptosis in nasopharyngeal carcinoma. *Cell Death Dis* 2018; 9. doi:10.1038/s41419-018-0265-y
 24. Aryankalayil MJ, Chopra S, Makinde A, et al. Microarray analysis of miRNA expression profiles following whole body irradiation in a mouse model. *Biomarkers* 2018; 23:689–703. doi:10.1080/1354750X.2018.1479771
 25. Menon N, Rogers CJ, Lukaszewicz AI, et al. Detection of acute radiation sickness: A feasibility study in non-human primates circulating miRNAs for triage in radiological events. *PLoS One* 2016; 11:1–18. doi:10.1371/journal.pone.0167333
 26. Fendler W, Malachowska B, Meghani K, et al. Evolutionarily conserved serum microRNAs predict radiation-induced fatality in nonhuman primates. *Sci Transl Med* 2017; 9:1–12. doi:10.1126/scitranslmed.aal2408
 27. Templin T, Amundson SA, Brenner DJ, et al. Whole mouse blood microRNA as biomarkers for exposure to γ -rays and ^{56}Fe ions. *Int J Radiat Biol* 2011; 87:653–62. doi:10.3109/09553002.2010.549537
 28. Acharya SS, Fendler W, Watson J, et al. Serum microRNAs are early indicators of survival after radiation-induced hematopoietic injury. *Sci Transl Med* 2015; 7:287ra69. doi:10.1126/scitranslmed.aaa6593
 29. Yadav M, Bhayana S, Liu J, et al. Two-miRNA-based finger-stick assay for estimation of absorbed ionizing radiation dose. *Sci Transl Med* 2020; 12:1–15. doi:10.1126/scitranslmed.aaw5831
 30. Coleman C, Koerner JF. Biodosimetry: Medicine, science, and systems to support the medical decision-maker following a large scale nuclear or radiation incident. *Radiat Prot Dosimetry* 2016; 172:38–46. doi:10.1093/rpd/ncw155
 31. Aryankalayil MJ, Chopra S, Levin J, et al. Radiation-Induced Long Noncoding RNAs in a Mouse Model after Whole-Body Irradiation. *Radiat Res* 2018; 189:251. doi:10.1667/rr14891.1
 32. Miyamoto T, Akutsu SN, Tauchi H, et al. Exploration of genetic basis underlying individual differences in radiosensitivity within human populations using genome editing technology. *J Radiat Res* 2018; 59:ii75–82. doi:10.1093/JRR/RRY007
 33. Alsbeih G, Al-Harbi N, Ismail S, et al. Impaired DNA Repair Fidelity in a Breast Cancer Patient with Adverse Reactions to Radiotherapy. *Front Public Health* 2021; 9:568. doi:10.3389/FPUBH.2021.647563/BIBTEX
 34. Grahm D, Hamilton KF. Genetic Variation in the Acute Lethal Response of Four Inbred Mouse Strains to Whole Body X-Irradiation. *Genetics* 1957; 42:189-198.
 35. Ao X, Zhao L, Davis MA, et al. Radiation produces differential changes in cytokine profiles in radiation lung fibrosis sensitive and resistant mice. *J Hematol Oncol* 2009 2:1 2009; 2:1–12. doi:10.1186/1756-8722-2-6
 36. Rivina L, Davoren MJ, Schiestl RH. Mouse models for radiation-induced cancers. *Mutagenesis* 2016; 31:491–509. doi:10.1093/MUTAGE/GEW019
 37. Rudqvist N, Laiakis EC, Ghandhi SA, et al. Global Gene Expression Response in Mouse Models of DNA Repair Deficiency after Gamma Irradiation. *Radiat Res* 2018; 189:337. doi:10.1667/rr14862.1
 38. Suresh Kumar MA, Laiakis EC, Ghandhi SA, et al. Gene Expression in Parp1 Deficient Mice Exposed to a Median Lethal Dose of Gamma Rays. *Radiat Res* 2018; 190:53. doi:10.1667/rr14990.1
 39. Sproull M, Shankavaram U, Camphausen K. Comparison of Proteomic Biodosimetry Biomarkers Across Five Different Murine Strains. *Radiat Res* 2019; 192:640. doi:10.1667/rr15442.1
 40. Rogers CJ, Lukaszewicz AI, Yamada-Hanff J, et al. Identification of miRNA signatures associated with radiation-induced late lung injury in mice. *PLoS One* 2020; 15:1–18. doi:10.1371/journal.pone.0232411
 41. R Core Team. R: A language and environment for statistical computing. 2018.
 42. Benjamini Y, Hochberg Y. Controlling the False Discovery Rate : A Practical and Powerful Approach to Multiple Testing *J Royal Stat Soc Series B (Methodological)*, 1995; 57:289–300.
 43. Vlachos IS, Zagganas K, Paraskevopoulou MD, et al. DIANA-miRPath v3.0: Deciphering microRNA function with experimental support. *Nucleic Acids Res* 2015; 43:W460–6. doi:10.1093/nar/gkv403
 44. Breiman L. *Classification and Regression Trees*. Wadsworth, New York. Chapman and Hall 1984. <https://doi.org/10.1201/9781315139470>
 45. Xiang M, Zeng Y, Yang R, et al. U6 is not a suitable endogenous control for the quantification of circulating microRNAs. *Biochem Biophys Res Commun* 2014; 454:210–4. doi:10.1016/j.bbrc.2014.10.064
 46. Aryankalayil MJ, Chopra S, Makinde A, et al. Microarray analysis of miRNA expression profiles following whole body irradiation in a mouse model. *Biomarkers* 2018; 23:689–703. doi:10.1080/1354750X.2018.1479771
 47. Natarajan V. Regulation of DNA repair by non-coding miRNAs. *Noncoding RNA Res*. 2016; 1:64–8. doi:10.1016/j.ncrna.2016.10.002
 48. Wang Y, Taniguchi T. MicroRNAs and DNA damage response: Implications for cancer therapy. *Cell Cycle*. 2013; 12:32–42. doi:10.4161/cc.23051
 49. Bian H, Zhou Y, Zhou D, et al. The latest progress on miR-374 and its functional implications in physiological and pathological processes. *J Cell Mol Med*. 2019; 23:3063–76. doi:10.1111/jcmm.14219
 50. Rogers CJ, Kyubwa EM, Lukaszewicz AI, Yamada-Hanff J, Starbird MA, Miller TA, et al. N Identification of miRNA Associated with Reduced Survival after Whole-Thorax Lung Irradiation in Non-Human Primates. *Radiat Res* 2021; 196:510-22.
 51. Kamath AB, Alt J, Debbabi H, et al. Toll-like receptor 4-defective C3H/HeJ mice are not more susceptible than other C3H substrains to infection with *Mycobacterium tuberculosis*. *Infect Immun* 2003; 71:4112–8. doi:10.1128/IAI.71.7.4112-4118.2003
 52. Bhogal N, Kaspler P, Jalali F, et al. Late residual γ -H2AX foci in murine skin are dose responsive and predict radiosensitivity in vivo. *Radiat Res* 2010; 173:1–9. doi:10.1667/RR1851.1
 53. Rube CE, Grudzenski S, Kühne M, et al. DNA double-strand break repair of blood lymphocytes and normal tissues analysed in a preclinical mouse model: Implications for radiosensitivity testing. *Clin Cancer Res* 2008; 14:6546–55. doi:10.1158/1078-0432.CCR-07-5147
 54. Haston CK. Mouse genetic approaches applied to the normal tissue radiation response. *Front Oncol*. 2012; 2 AUG. doi:10.3389/fonc.2012.00094
 55. Peraza-Vega RI, Valverde M, Rojas E. Interactions between miRNAs and Double-Strand Breaks DNA Repair Genes, Pursuing a Fine-Tuning of Repair. *Int J Mol Sci*. 2022; 23. doi:10.3390/ijms23063231
 56. Kriegel AJ, Liu Y, Fang Y, et al. The miR-29 family: genomics, cell biology, and relevance to renal and cardiovascular injury. *Physiol Genomics* 2012; 44:237–44. doi:10.1152/physiolgenomics.00141.2011

57. Kim H, Ko Y, Park H, et al. MicroRNA-148a/b-3p regulates angiogenesis by targeting neuropilin-1 in endothelial cells. *Exp Mol Med* 2019; 51. doi:10.1038/s12276-019-0344-x
58. Zhou Z, Collado A, Sun C, et al. Downregulation of Erythrocyte miR-210 Induces Endothelial Dysfunction in Type 2 Diabetes. *Diabetes* 2022; 71:285–97. doi:10.2337/db21-0093
59. Pannkuk EL, Laiakis EC, Mak TD, et al. A Lipidomic and Metabolomic Serum Signature from Nonhuman Primates Exposed to Ionizing Radiation. *Metabolomics* 2016; 12:80. doi:10.1007/s11306-016-1010-0
60. Wong WM, Liao JJ, Laramore GE, et al. L-lysine in the Treatment of Oral Mucositis in Head-and-Neck Cancer Patients: A Pilot Study. *Int J Radiat Oncol Biol Phys* 2013; 87:S568. doi:10.1016/j.ijrobp.2013.06.1507
61. Rinschen MM, Palygin O, El-Meanawy A, et al. Accelerated lysine metabolism conveys kidney protection in salt-sensitive hypertension. *Nat Commun* 2022; 13. doi:10.1038/s41467-022-31670-0
62. Zhao F, Pu Y, Qian L, et al. MiR-20a-5p promotes radio-resistance by targeting NPAS2 in nasopharyngeal cancer cells. *Oncotarget* 2017; 8:105873–81. doi:10.18632/oncotarget.22411
63. Gao F, Liu P, Narayanan J, et al. Changes in miRNA in the lung and whole blood after whole thorax irradiation in rats. *Sci Rep* 2017; 7. doi:10.1038/srep44132
64. Martin-Alonso A, Cohen A, Quispe-Ricalde MA, et al. Differentially expressed microRNAs in experimental cerebral malaria and their involvement in endocytosis, adherens junctions, FoxO and TGF- β signalling pathways. *Sci Rep* 2018; 8. doi:10.1038/s41598-018-29721-Y
65. Su S, Zhao Q, He C, et al. miR-142-5p and miR-130a-3p are regulated by IL-4 and IL-13 and control profibrogenic macrophage program. *Nat Commun* 2015; 6. doi:10.1038/NCOMMS9523
66. Nunamaker EA, Artwohl JE, Anderson RJ, et al. Endpoint Refinement for Total Body Irradiation of C57BL/6 Mice. 2013; *Comp Med* 63:22-28.
67. Cheda A, Nowosielska EM, Gebicki J, et al. A derivative of vitamin B3 applied several days after exposure reduces lethality of severely irradiated mice. *Sci Rep* 2021; 11. doi:10.1038/s41598-021-86870-3
68. Zhang C, Ni J, Gao F, et al. The mechanism for the ameliorative effect of CpG-oligodeoxynucleotides on bone marrow hemopoiesis radiation injury. *Basic Clin Pharmacol Toxicol* 2011; 109: 11–6. doi:10.1111/j.1742-7843.2011.00695.x
69. Chakraborty N, Gautam A, Holmes-Hampton GP, et al. microRNA and Metabolite Signatures Linked to Early Consequences of Lethal Radiation. *Sci Rep* 2020; 10. doi:10.1038/s41598-020-62255-w
70. Hong LZ, Zhou L, Zou R, et al. Systematic evaluation of multiple qPCR platforms, NanoString and miRNA-Seq for microRNA biomarker discovery in human biofluids. *Sci Rep* 2021; 11. doi:10.1038/s41598-021-83365-z
71. Crossland RE, Norden J, Juric MK, et al. Expression of serum microRNAs is altered during acute graft-versus-host disease. *Front Immunol* 2017; 8. doi:10.3389/fimmu.2017.00308
72. Foye C, Yan IK, David W, et al. Comparison of miRNA quantitation by Nanostring in serum and plasma samples. *PLoS One* 2017; 12. doi:10.1371/journal.pone.0189165
73. Tsang HF, Xue VW, Koh SP, et al. NanoString, a novel digital color-coded barcode technology: current and future applications in molecular diagnostics. *Expert Rev Mol Diagn*. 2017; 17: 95–103. doi:10.1080/14737159.2017.1268533
74. Pescarmona R, Belot A, Villard M, et al. Comparison of RT-qPCR and Nanostring in the measurement of blood interferon response for the diagnosis of type I interferonopathies. *Cytokine* 2019; 113:446–52. doi:10.1016/j.cyto.2018.10.023
75. Patterson AM, Plett PA, Chua HL, et al. Development of a Model of the Acute and Delayed Effects of High Dose Radiation Exposure in Jackson Diversity Outbred Mice; Comparison to Inbred C57BL/6 Mice. *Health Phys* 2020; 119:633–46. doi:10.1097/HP.0000000000001344
76. Okayasu R, Suetomi K, Yu Y, et al. A Deficiency in DNA Repair and DNA-PKcs Expression in the Radiosensitive BALB/c Mouse. *Cancer Res* 2000; 60:4342-5.
77. Cross KM, Granados JZ, Ten Have GAM, et al. Protein fractional synthesis rates within tissues of high- and low-active mice. *PLoS One* 2020; 15:e0242926. doi:10.1371/JOURNAL.PONE.0242926
78. Barrios M, Rodríguez-Acosta A, Gil A, et al. Comparative hemostatic parameters in BALB/c, C57BL/6 and C3H/He mice. *Thromb Res* 2009; 124:338–43. doi:10.1016/J.THROMRES.2008.11.001
79. Wiedmeyer B, To J, Sridharan DM, et al. Dose Fractionation During Puberty Is More Detrimental to Mammary Gland Development Than an Equivalent Acute Dose of Radiation Exposure. *International J Radiat Oncol Biol Phys* 2021; 109: 1521–32. doi:10.1016/J.IJROBP.2020.11.039